

Isospin Fluctuations from Multiple Domains of Disoriented Chiral Condensate

James Hormuzdiar*

Department of Physics, Yale University, New Haven, CT 06520-8120

Stephen D.H. Hsu[†]

Department of Physics, University of Oregon, Eugene, OR 97403-5203

February, 1998

Abstract

We describe some detailed numerical simulations of Disoriented Chiral Condensates (DCCs), using the chiral lagrangian as a controlled long-wavelength description. We focus on the possibility of multiple, independently coherent domains, and investigate the degree to which the DCC signal is attenuated. As an intermediate step in our analysis we compute the expected number of detector events in each isospin and momentum channel for a given asymptotic classical field configuration. We find that for sufficiently large initial field strengths, the non-linear interactions between domains become important and can lead to a randomization of isospin orientations. Nevertheless, we argue that viable signals exist for DCC detection, even in the case of multiple domains and strong domain-domain interactions. We briefly discuss some long-lived ‘pseudo-bound state’ configurations which arise at large field strengths and might be observable in HBT correlations.

*james.hormuzdiar@yale.edu

[†]hsu@duende.uoregon.edu

1 Introduction

One of the most exciting possibilities at RHIC is that collisions of heavy nuclei might lead to coherent, pion field configurations which are produced by the disorientation of the chiral condensate (DCC) [1, 2, 3, 4, 5] (for recent review articles, see [6, 7]). Such coherent configurations could lead to large, characteristic fluctuations in the number and type of pions measured in detectors. Unfortunately, the evolution of quantum fields in the aftermath of the heavy ion collision is a difficult problem, involving both strong coupling effects and non-equilibrium statistical mechanics, and remains to be solved despite much theoretical effort. Most previous work has been performed in the context of the linear sigma model, sometimes using an approximation like the $1/N$ expansion to control the quantum corrections [8]–[19]. However, the relationship between linear sigma model dynamics and real QCD dynamics is unclear.

Our approach here will be somewhat different. We adopt an agnostic approach to the *formation* of DCCs, and simply try to characterize their evolution at subsequent times, with an eye toward experimental signatures. We make a detailed investigation of the phenomenology of DCCs using the classical field equations derived from the chiral lagrangian (non-linear sigma model) to describe their evolution from initial domain(s) to the final state which arrives in the detector. The field equations of the chiral lagrangian can be organized in a momentum expansion, and therefore yield a controlled approximation for sufficiently slowly-varying pionic configurations. While this approach has no advantages for the formation problem, it does provide a way of simulating, in a controlled fashion, the subsequent evolution of domains once formed. Indeed, quantum corrections (loop effects) are suppressed as long as the configurations simulated are sufficiently “soft” relative to the scale $4\pi F_\pi \simeq 1 \text{ GeV}$. We verify that this treatment is self-consistent: initially soft configurations do not lead to the build up of hard sub-configurations which cannot be treated within the chiral lagrangian.

We will be particularly interested in the possibility of multiple coherent domains, since it seems unlikely that a single large domain would remain in the wake of the collision [13, 14, 17]. Therefore, we simulate the interactions between domains with different initial isospin orientations. For sufficiently weak fields, interactions can be neglected, leading to particle distributions which are simply linear superpositions of those expected from each separate domain. In this case the effect of N multiple domains is mainly “statistical”, leading to a narrower width (proportional to $1/\sqrt{N}$) in fluctuations. However, at sufficiently large field strengths, which we quantify below (but which are well within the roughly expected range), the interactions are significant and have a strong effect on the field configurations, even if the number of domains is small. Our results are discussed in detail below, however the general observation one can make is that non-linearities can degrade the DCC signal, leading to a

somewhat narrower distribution in fluctuations of the charge ratios. Despite this, we find that promising signals of multiple DCC domain formation remain even in the non-linear cases. We also briefly discuss some interesting ‘pseudo-bound state’ (PBS) configurations which appear at large field strengths. These configurations have particularly long lifetimes and might be observable in HBT correlations at RHIC.

The organization of this paper is as follows. In section 2 we review the chiral lagrangian approximation to low-energy QCD, and derive the corresponding classical field equations. In section 3 we discuss various aspects of multiple domains, including the straightforward statistical analysis. In section 4 we describe our simulation and our numerical results, including details of the non-linear behavior. In section 5 we present our conclusions. Appendices A, B and C contain some useful formulae, as well as a description of our “detector” subroutine and of how isospin rotations of our configurations were performed. In appendix D we give additional details concerning the simulations and the parameters used.

2 Chiral Lagrangian Description

The chiral lagrangian is the most general effective lagrangian consistent with the symmetries of low energy QCD [20]. As such, it accurately describes the soft dynamics of pseudo-Goldstone mesons, including the virtual effects of heavier particles such as baryons, the rho meson, etc. which have already been integrated out. We can classify the possible terms by the number of derivatives, with the first term given by

$$\mathcal{L} = \frac{F_\pi^2}{4} \text{tr}(\partial^\mu \Sigma^\dagger \partial_\mu \Sigma) \quad (1)$$

where

$$\Sigma = e^{i\vec{\pi} \cdot \vec{\tau} / F_\pi} . \quad (2)$$

The effects of higher order terms are proportional to powers of the momentum, as are any quantum loop effects calculated with (1). This implies that for sufficiently soft configurations, the classical field equations derived from (1) describe the full quantum mechanical evolution. For this reason, we believe that the chiral lagrangian is superior to the usual linear sigma model for studying the dynamics of DCC’s, at least after formation. Our approximation relies on a momentum expansion, rather than $1/N$ or Hartree-Fock.

We define a four component real field $\phi = (\sigma, \vec{\phi})$ such that $F_\pi \Sigma = \sigma I + i\vec{\tau} \cdot \vec{\phi}$ with the condition $\phi^2 = F_\pi^2$ everywhere. It is clear that we can do this, since

$$e^{i\vec{\tau} \cdot \vec{A}} = \cos(|\vec{A}|)I + i \frac{\vec{\tau} \cdot \vec{A}}{|\vec{A}|} \sin(|\vec{A}|) . \quad (3)$$

In terms of ϕ , we have

$$\mathcal{L} = \frac{1}{2} \partial^\mu \phi \cdot \partial_\mu \phi \quad , \quad (4)$$

with the condition $\phi^2 = F_\pi^2$.

Rather than deal with the complicated constrained equations which result from (4), we relax the condition on ϕ^2 slightly by replacing it with a potential term in the lagrangian whose minimum falls at $\phi^2 = F_\pi^2$. This yields the linear sigma model with potential

$$V(\phi) = \frac{\lambda}{4} [\phi^2 - F_\pi^2]^2, \quad (5)$$

and lagrangian

$$\mathcal{L} = \frac{1}{2} \partial^\mu \phi \cdot \partial_\mu \phi - V(\phi) = \frac{1}{2} \partial^\mu \phi \cdot \partial_\mu \phi - \frac{\lambda}{4} [\phi^2 - F_\pi^2]^2 \quad . \quad (6)$$

The limiting case $\lambda \rightarrow \infty$ yields the original non-linear sigma model.

In reality, the chiral symmetry is slightly broken by bare quark masses, resulting in non-zero pion masses. Taking this into account yields

$$\mathcal{L} = \frac{1}{2} \partial^\mu \phi \cdot \partial_\mu \phi - \frac{\lambda}{4} [\phi^2 - F_\pi^2]^2 - \frac{m_\pi^2}{2} (\phi^2 - 2F_\pi \sigma + F_\pi^2). \quad (7)$$

This lagrangian yields the classical equations of motion

$$\partial^2 \vec{\phi} = -[\lambda(\phi^2 - F_\pi^2) + m_\pi^2] \vec{\phi} \quad (8)$$

$$\partial^2 \sigma = -[\lambda(\phi^2 - F_\pi^2) + m_\pi^2] \sigma + m_\pi^2 F_\pi \quad . \quad (9)$$

In the non-linear sigma model limit we wish to consider, σ is just F_π plus a very small quantity. Because floating point variables do not deal well with this arrangement, it is more useful to redefine $\sigma \rightarrow \tilde{\sigma} + F_\pi$, with equations of motion

$$\partial^2 \vec{\phi} = -[\lambda(\tilde{\phi}^2 + 2F_\pi \tilde{\sigma}) + m_\pi^2] \vec{\phi} \quad (10)$$

$$\partial^2 \tilde{\sigma} = -[\lambda(\tilde{\phi}^2 + 2F_\pi \tilde{\sigma}) + m_\pi^2] \tilde{\sigma} - \lambda(\tilde{\phi}^2 + 2F_\pi \tilde{\sigma}) F_\pi.$$

3 Multiple Domains

A telltale sign of DCC formation would be large fluctuations in pion isospin abundances. Under incoherent production of hundreds or possibly thousands of pions, one would expect nearly equal numbers of each type to be emitted, whereas with coherent DCC domains, the abundances would be a function of the domain isospin orientation. If one domain happened

to point in the π_0 direction, then each of the outgoing pions would be a π_0 , an improbable occurrence under incoherent production. In the case of a single, coherent domain, the exact probability distribution for

$$f \equiv \frac{N_{\pi^0}}{N_{\pi^0} + N_{\pi^+} + N_{\pi^-}} \quad (11)$$

is easily seen to be $dP(f) = df/2\sqrt{f}$.

The case of k multiple domains is more complicated, but in the low field strength approximation it can be simplified by the neglect of interactions, so that the distribution of pions is the sum of the distribution from each single domain. If the size of each domain is taken to be roughly the same, and hence total particle output $N = N_{\pi^0} + N_{\pi^+} + N_{\pi^-}$ does not differ from domain to domain, then the total f is simply the average of that for the individual domains,

$$f_{total} = \frac{\sum N_{\pi^0}^j}{\sum N_j} = \frac{\sum N_{\pi^0}^j}{kN} = \frac{1}{k} \sum f^j \quad (12)$$

As was also shown in [21], the distribution for this total f can now be computed as a function of k . Analytical results are difficult to obtain, but by randomly generating domain orientations (with a flat probability distribution on the three sphere), the probability distribution curves can be calculated numerically. By generating large quantities of samples, the error bars in the distribution curves were lowered enough to be negligible in the graphs, approximating the limiting case of a continuum probability distribution. Figure 1 shows the behavior of $P(f)$ for increasing values of k .

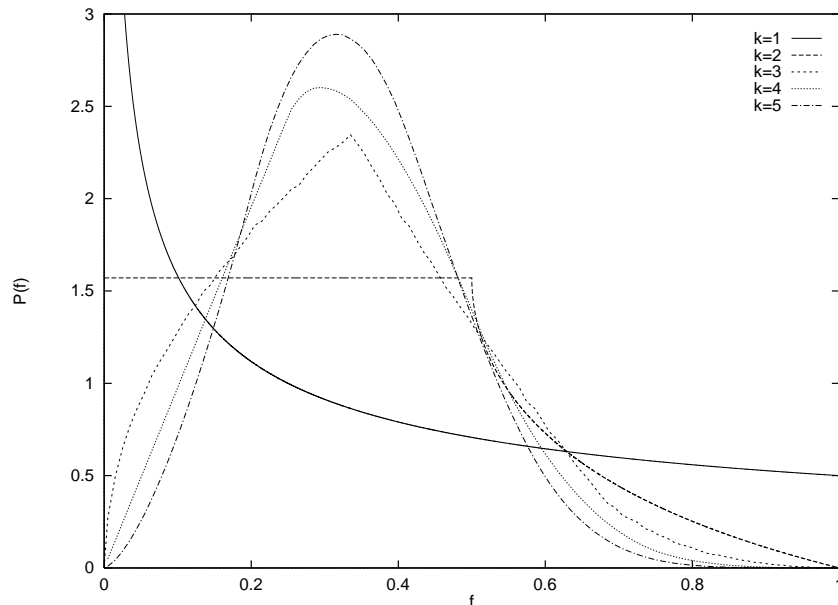


Figure 1: Probability distribution of f [$P(f)$] for varying k

The general behavior is a result of the central limit theorem, which tells us that as statistical sampling is performed repeatedly, the average value of the resultant variable stays the same, while its standard deviation is proportional to $1/\sqrt{k}$. The proportionality constant is easy to fix by calculating the standard deviation for the $k = 1$ case, whose probability distribution was given above as $dP(f) = df/2\sqrt{f}$. This yields

$$\sigma_{\text{coherent}} \equiv \sqrt{\langle f^2 \rangle - \langle f \rangle^2} = \frac{2}{3\sqrt{5k}} \quad . \quad (13)$$

We can repeat this calculation for the incoherent case with N particles emitted, using the probability distribution for single particle production,

$$P(f) = \frac{2}{3}\delta(f) + \frac{1}{3}\delta(f - 1).$$

In this case

$$\sigma_{\text{incoherent}} = \frac{1}{3}\sqrt{\frac{2}{N}} \quad . \quad (14)$$

While we do not know precisely how many domains (if any!) are likely to be formed in a typical collision, it is difficult to imagine that k is much larger than of order 10 or so, simply due to the restricted geometry of the collision region. Therefore, N is likely to be large compared to k and there is still a significant qualitative difference between the distribution of results from incoherent and coherent production. The overall level of fluctuations in f should be larger in the coherent case. Whether this difference could be observed at RHIC depends of course on the probability of DCC formation per collision.

The coherent analysis would be modified if some fraction a of the outgoing pions were assumed to be produced by incoherent background processes. For $(N'_{\pi_0}, N'_{\pi_+}, N'_{\pi_-})$ coherently produced and $(N''_{\pi_0}, N''_{\pi_+}, N''_{\pi_-})$ incoherently produced pions, (where $N''_{\text{total}} = a(N'_{\text{total}} + N''_{\text{total}})$), the value of f is (neglecting effects of order $1/\sqrt{N''}$)

$$f = \frac{N'_{\pi_0} + N''_{\pi_0}}{N'_{\text{total}} + N''_{\text{total}}} = (1 - a)f_{\text{non-corrupted}} + \frac{1}{3}a \quad . \quad (15)$$

Using this the standard deviation of f becomes

$$\sigma_{\text{coherent}} = (1 - a)\frac{2}{3\sqrt{5k}} \quad . \quad (16)$$

Hence incoherent corruption narrows the spread in f around $1/3$.

In the above discussion we ignored the interactions between the coherent configurations. Clearly this is justified for sufficiently weak fields, but when the pion field strengths are large the interactions between different domains can be significant. It is well known that

the solution of classical field equations is equivalent to the resummation of all tree graphs in perturbation theory. Nonlinearities in the classical field evolution therefore represent large rescattering effects due to tree-level vertices. As mentioned previously, all loop graphs in chiral perturbation theory contain extra powers of the external momentum squared, and are hence suppressed. We expect rescattering to be important when the pion number densities are sufficiently large. The effect of the interactions is not clear *a priori*, although one might argue that they tend to randomize the isospin orientations and lead to smaller, not larger, fluctuations in f for a fixed number of domains. To gain some insight on this question, we performed numerical simulations of domain-domain interactions using the low energy effective field theory described in the previous section.

In our simulations we allowed the field strengths to vary in the range of $|\vec{\pi}| \sim F_\pi$. Due to our lack of control over the formation process, we are unable to compute with any precision the expected number or energy density of pions in the DCC. However, a simple estimate based on a critical temperature of chiral symmetry restoration $T_c \simeq 200$ MeV, and the assumption that the energy density of pions in the DCC is roughly that of the hadron gas at T_c , yields field strengths as large as $(4-5) F_\pi$. As we will see below, the evolution of multiple domains is significantly non-linear at field strengths which are as small as $|\vec{\pi}| \simeq 1.4 F_\pi$.

4 Simulation and Results

We performed simulations of domain-domain interactions in a cylindrical geometry with axial symmetry. The domains themselves are cylinders placed end to end along the beam axis, with domain walls in between. This is of course an idealization of the actual configuration, chosen for simplicity and to make our simulations tractable.

4.1 The Difference Equation

A computer simulation written in C++ was used to evolve eq. (10). Imposing axial symmetry, the left side of the equation becomes

$$\partial^2 \phi = \frac{\partial^2 \phi}{\partial t^2} - \frac{\partial^2 \phi}{\partial z^2} - \frac{1}{r} \frac{\partial}{\partial r} \left[r \frac{\partial \phi}{\partial r} \right] = \frac{\partial^2 \phi}{\partial t^2} - \frac{\partial^2 \phi}{\partial z^2} - \frac{1}{r} \frac{\partial \phi}{\partial r} - \frac{\partial^2 \phi}{\partial r^2} . \quad (17)$$

Defining a discrete function

$$\phi_{i,j,k} \equiv \phi(i\Delta t, j\Delta r, k\Delta z), \quad (18)$$

and using the following finite-difference approximations

$$\frac{\partial \phi}{\partial q} \simeq \frac{\phi_{i+1} - \phi_{i-1}}{2\Delta q} \quad (19)$$

$$\frac{\partial^2 \phi}{\partial q^2} \simeq \frac{\phi_{i+1} - 2\phi_i + \phi_{i-1}}{\Delta q^2} , \quad (20)$$

the equations of motion become

$$\begin{aligned} \phi_{i+1,j,k} = & 2\left(1 - 2\frac{\Delta t^2}{\Delta z^2}\right)\phi_{i,j,k} + \frac{\Delta t^2}{\Delta z^2}\left[\left(1 + \frac{1}{2j}\right)\phi_{i,j+1,k} \right. \\ & \left. + \left(1 - \frac{1}{2j}\right)\phi_{i,j-1,k} + F_{i,j,k+1} + F_{i,j,k-1}\right] - F_{i-1,j,k} + \Delta t^2 G(\phi_{i,j,k}) . \end{aligned} \quad (21)$$

(Here $\Delta r = \Delta z$, and $G(\phi_{i,j,k})$ is the expression on the right hand side of the original equation).

By storing the two previous time slices of the field ($\phi_{i,j,k}$ and $\phi_{i-1,j,k}$), the newer value ($\phi_{i+1,j,k}$) can be calculated, allowing for the time evolution of the fields given an initial configuration and its time derivative.

4.2 Initial Configurations

An initial configuration is described by its number of domains k , their positions, sizes, field strengths, and isospin orientations. For simplicity we assume the size and strength of each domain is the same (owing to a similarity in formation processes). We also choose the field configurations of the first two timeslices to be the same. As a final simplifying assumption we have ignored the initial expansion velocities of the domains. Such velocities would probably *decrease* the nonlinear effects, since the pions would disperse more rapidly to low densities.

Distinct fixed values of k are treated differently.

k=1

Here the initial conditions for each run are characterized by one vector \vec{v} representing the orientation and strength of the single domain in isospace.

Varying the field strength in the $k=1$ case yields no change in the distribution curve for f . It can be easily shown (e.g., using the results in appendix C) that the final values of N_{π_0} , N_{π_+} , and N_{π_-} are proportional to the square of the three components of \vec{v} :

$$(N_{\pi_0}, N_{\pi_+}, N_{\pi_-}) \propto (v_{\pi_0}^2, v_{\pi_+}^2, v_{\pi_-}^2) . \quad (22)$$

The proportionality constant cancels out in the definition of f , leaving it and its statistics invariant to the initial strength.

k=2

The initial configurations for the $k=2$ case can be parameterized by two isospin vectors \vec{v}_1 and \vec{v}_2 . To generate the $P(f)$ curves, the field strength of the two domains was fixed at

the given value $|\vec{v}_1| = |\vec{v}_2| = s$, multiple runs with random orientations were performed, and the resulting f 's were binned, much like in the weakly interacting case.

Each run requires tens of minutes, hence it is too time consuming to perform the $O(10^9)$ simulations needed to smooth the probability curves. Instead, the rotational techniques developed in appendix C were exploited, and the simulation was only run for \vec{v}_1 and \vec{v}_2 orientations in the $\pi_0 - \pi_+$ plane, symmetric around the π_0 axis. Rotating this representative class yields all possible initial configurations.

The actual functional shape of the initial field configurations is specified by a magnitude and angular dependence. The magnitude is given by

$$|\vec{\pi}(r, z)| = s * g(|z|)g(r) , \quad (23)$$

with $g(x) = 1 / (1 + e^{k_1(x-a)})$. This function (for appropriate k_1 's) is nearly constant for $x < a$, drops suddenly at $x \simeq a$, then stays approximately 0 for $x > a$. The angular dependence, measured in the $\pi_0 - \pi_+$ plane from the π_0 axis, is

$$\angle \vec{\pi}(r, z) = \frac{2}{\pi} \alpha \arctan(k_2 z) , \quad (24)$$

which plateaus to $+\alpha$ for $z > 0$ and $-\alpha$ for $z < 0$. These equations describe a cylinder centered at $z = r = 0$ subdivided into a $z > 0$ part with isospin in the $+\alpha$ direction and a $z < 0$ part with isospin in the $-\alpha$ direction. Values of k_1 , k_2 , and a were chosen to fix the physical dimensions. Each isospin region has a height and diameter of 10 fm, with a 'skin' thickness of 1 fm. (The 'skin' is defined as the region where the field amplitude drops from 90% to 10% of its maximum value.) Additional details of the computational techniques used in the simulations can be found in appendix D.

Figure 2 gives sample time snapshots in the evolution of the pion fields, where light white (dark black) corresponds to the maximum (minimum) value on the field in the given snapshot. Runs were continued until the Klein-Gordon Number Operator converged, signaling that the field had spread out far enough that the nonlinear terms had become negligible.

The progression of $P(f)$ for various initial field strengths was constructed and is shown in figure 3. The dotted line shows the low field strength approximation. Successive curves are then shown for initial field strengths of $0.01F_\pi$, $0.5F_\pi$, $1.0F_\pi$, $1.3F_\pi$, $1.4F_\pi$, $1.5F_\pi$, and $1.6F_\pi$. The trend towards a more randomized probability distribution is apparent, although the width of the distribution and the area under the tails (in particular, $f \simeq 1$) is not changed significantly. One way to understand this is to note that in order to get an event with f close to unity, the initial domains must all be oriented in the same direction. This is of course less and less probable as the number of domains k gets larger, but once the domains are formed in this way the common orientation suppresses their interactions – in

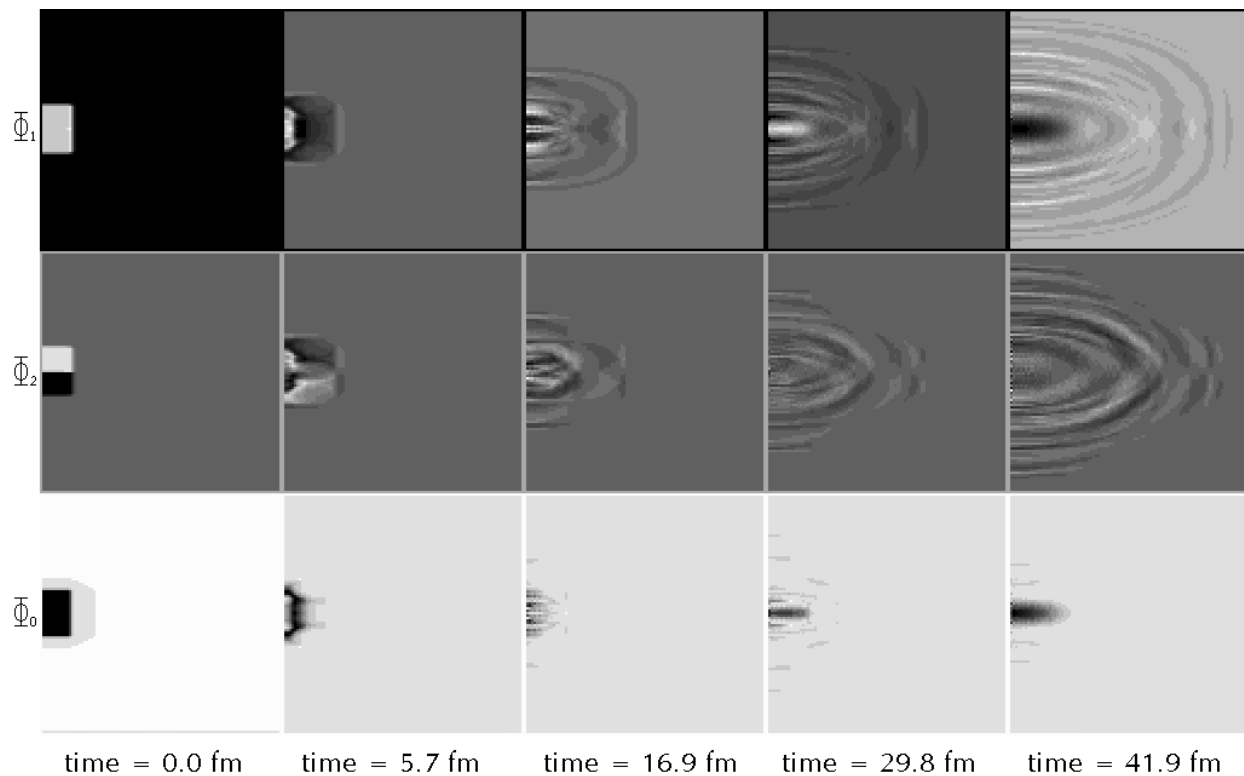


Figure 2: Numerical evolution of the fields

other words they act like one big domain. Thus we expect the number of $f \simeq 1$ events to be preserved even at large field strengths.

$k > 2$

Computational power limited our ability to do an exhaustive analysis of the $k > 2$ case. For the $k=3$ case, initial configurations are parameterized by the three unit vectors and an overall strength. Even exploiting the rotational symmetry and fixing field strength, three free parameters remain. Building a representative class of configurations, sampling each variable at S values would need at least S^3 computer runs. Even the marginally acceptable value of $S = 10$ would require 1000 runs, which at greater than 2 hours per run on our DEC Alpha Workstation would require almost 3 months. Although more powerful computers could be assigned to this task, we feel that the important qualitative features of the domain to domain interaction are already featured in the $k=2$ case. This intuition is based in part on the (explicitly confirmed) observation that when two domains are separated from each other at larger distances, interactions become quickly negligible. Thus, in the case of k domains arranged colinearly (as required by the axial symmetry) only the nearest neighbor domain walls would interact significantly. Of course this single domain wall was well studied in the

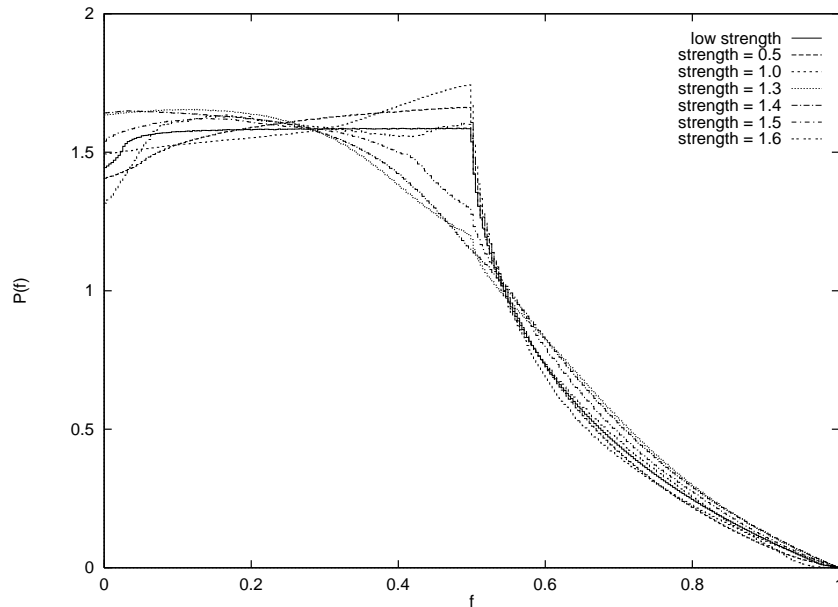


Figure 3: Probability distribution of f [$P(f)$] for varying field strength

k=2 case.

4.3 Nonlinearities and Pseudo-Bound States

Increasing the strength of the field configurations qualitatively changes the evolution of the fields. We carefully examined the runs to determine the critical amplitude at which nonlinearities set in. In these observations a surprising behavior was noticed. For values of initial strengths between 0 and $1.2F_\pi$, evolution proceeded similarly to the non-interacting case. However, for slightly higher field strengths we observed that a large fraction of the energy bunched up in the central region and held together for long periods of time. Figure 4 shows the energy in a 10 fm spherical region centered around the origin vs. time. As can be seen in these graphs, once the threshold has been crossed a pseudo-bound state forms.

This phenomenon was found to be robust: it was replicated in runs in which the initial conditions were varied. We also studied the evolution of spherically symmetric configurations using separately written code. Again, once a certain initial strength was crossed, the configuration held together in a pseudo-bound state for much longer periods of time. It is in fact the long evolution times required for the configuration to completely disperse that limited our ability to compute the probability distribution in f beyond the $1.6F_\pi$ case.

These much longer dispersion times are potentially observable in HBT (Hanbury Brown-

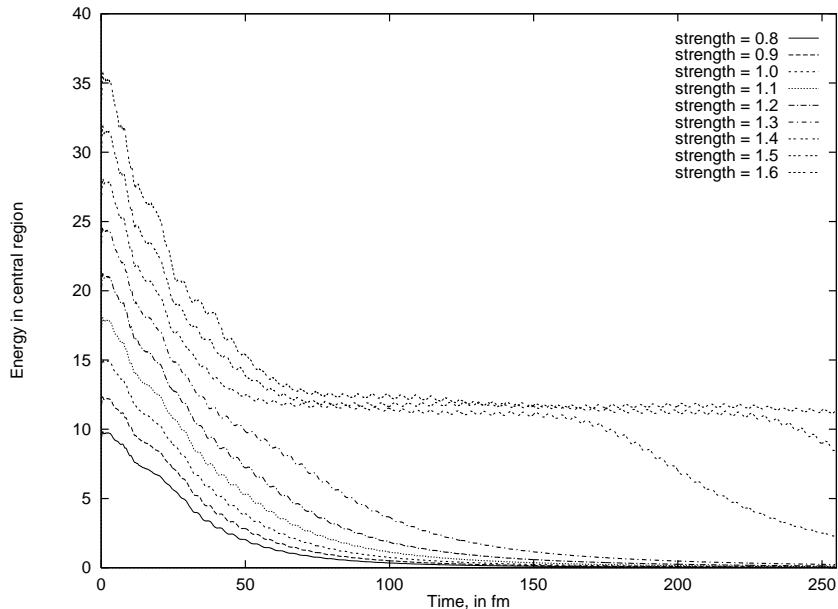


Figure 4: Central energy vs. time

Twiss) correlations¹. (For a recent review of these techniques, see [22].) Pseudo-bound state dispersion times as long as $10^{-22}s$ (versus $10^{-24}s$ for the noninteracting case) were observed, and we have every indication that longer lifetimes are possible. We intend to report in more detail on PBS dynamics in future work.

We note that although the configurations evolved very differently for higher field strengths, the $P(f)$ curves were only slightly modified. This fact leads us to assert that, at least up to the strengths that we were able to study, the noninteracting case remained a good approximation for the full evolution.

5 Signals

In this section we discuss two signals which can be used to detect or exclude DCC production. We focus on simple hypotheses with specific probabilities p_k for producing k domains of some fixed characteristic size.

¹We thank K. Rajagopal and D. Rischke for pointing this out to us.

5.1 Width Measurements

Purely incoherent pion production should yield a spread in values of f equal to $\sigma = \frac{1}{3}\sqrt{\frac{2}{N}}$ (equation 14). Any significant excess of this value would be strong evidence of DCC formation. Although the range of probable RHIC pion yields is presently unknown, experience from previous heavy ion collisions would suggest values in the hundreds or thousands, yielding $\sigma = 0.01$ to 0.05 , a range that would be surpassed for up to $k=35$ domains (equation 13).

In reality, k domain DCCs would be expected to form in only some fraction p_k of the events, yielding a smaller value of σ . Data can place upper bounds on each value of p_k from the following analysis. Assuming that only k domain DCC's and incoherent events form (for some given k), the probability distribution curve for f becomes

$$P(f) = p_k P_{k\text{-domains}}(f) + (1 - p_k) P_{\text{incoherent}}(f) \quad , \quad (25)$$

hence

$$\begin{aligned} \sigma_{\text{measured}}^2 &= \int df (f - \langle f \rangle)^2 [p_k P_{k\text{-domains}}(f) + (1 - p_k) P_{\text{incoherent}}(f)] \quad (26) \\ &= p_k \sigma_{\text{coherent}}^2 + (1 - p_k) \sigma_{\text{incoherent}}^2 \quad . \end{aligned}$$

Using equations 13 and 14, and reintroducing incoherent background corruption discussed in section 3, we can obtain an upper limit of p_k

$$p_k \leq \frac{5}{2}k \left[\frac{9N\sigma_m^2 - 2}{2(1-a)^2N - 5k} \right] \quad (27)$$

Figure 5 shows a plot of numerically calculated values of width vs. initial field strength (for the $k = 2$ case). Despite the level of nonlinear activity that occurs at higher strengths, the width does not change more than 10%. Up to the range of simulated cases, the noninteracting case is a good approximation. For higher strengths, there is probably a trend toward somewhat smaller widths.

5.2 Counting Rare Events

Another feature of incoherent production is that the distribution of f peaks sharply at $1/3$, and is nearly zero elsewhere, yielding an exponentially small tail of events where f is close to either 0 or 1. From elementary statistics the distribution of f is

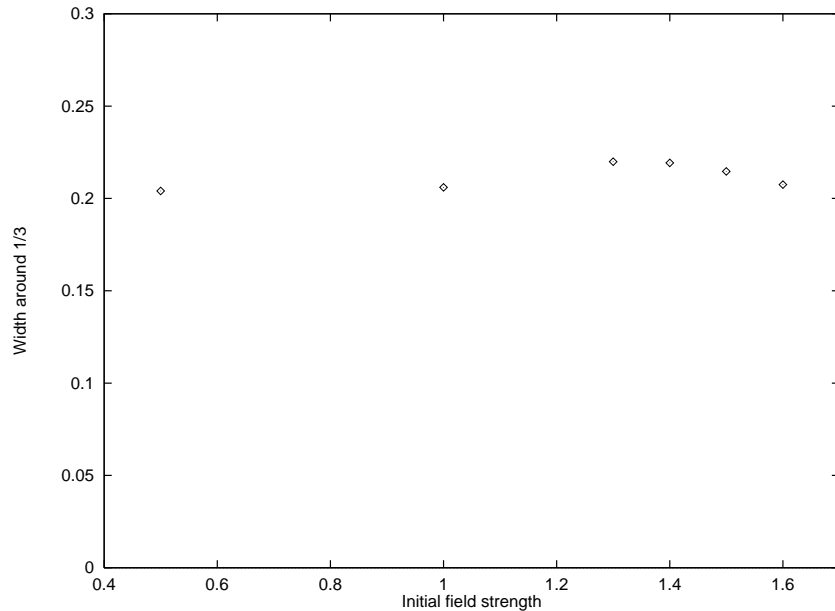


Figure 5: Standard deviation vs. initial field strength

$$P(f = i/N) = \binom{N}{i} \left(\frac{1}{3}\right)^i \left(\frac{2}{3}\right)^{N-i}. \quad (28)$$

where i is restricted to being an integer from 0 to N . Setting $N=100$ and integrating over the range $0.6 \leq f \leq 1$ yields the small value of 4.3×10^{-8} . Thus, given (for instance) 10^7 events, there is still only a 43% chance that $f \geq .6$ be measured even once.

A similar analysis for the coherent case was performed. For instance, with one domain, $P(f) = \frac{1}{2\sqrt{f}}$, for which 23% of the events lie above $f = 0.6$ (a much larger 2.3×10^6 of 10^7 assumed events). Now, assuming that only the incoherent and one domain coherent cases contribute, the fraction of rare events t would be

$$t = (1 - p_1) t' + p_1 t'' \quad (29)$$

where t' is the number of rare events expected from the incoherent case, t'' is the number from the coherent case, and p_1 is an element in the set of p_k 's introduced in the previous subsection. Presumably more than just these two cases would exist, so this equation sets an upper limit on p_1

$$p_1 \leq \frac{t - t'}{t'' - t'}. \quad (30)$$

In this manner, using the probability curves of f calculated in previous sections, data for other values of k were calculated. Table 1 shows the expected fraction of tail events for given

| Number of domains k | Fraction of events with $f > 0.6$ | Upper bound on $p_k(\leq \frac{t-t'}{t''-t'})$ |
|--|-----------------------------------|--|
| $k = 1$, all field strengths | 2.3×10^{-1} | $4.3 t - 1.9 \times 10^{-7}$ |
| $k = 1$, all field strengths \dagger | 1.8×10^{-1} | $5.4 t - 2.3 \times 10^{-7}$ |
| $k = 2$, Low field strengths | 1.2×10^{-1} | $8.3 t - 3.6 \times 10^{-7}$ |
| $k = 2$, Low field strengths \dagger | 7.4×10^{-2} | $14 t - 5.8 \times 10^{-7}$ |
| $k = 2$, High field strengths | 1.1×10^{-1} | $9.1 t - 3.9 \times 10^{-7}$ |
| $k = 2$, High field strengths \dagger | 7.1×10^{-2} | $14.1 t - 6.1 \times 10^{-7}$ |
| $k = 4$ | 5.0×10^{-2} | $20 t - 8.6 \times 10^{-7}$ |
| $k = 4 \dagger$ | 1.8×10^{-2} | $56 t - 2.4 \times 10^{-6}$ |
| $k = 8$ | 8.4×10^{-3} | $120 t - 5.1 \times 10^{-6}$ |
| $k = 8 \dagger$ | 1.4×10^{-3} | $710 t - 3.1 \times 10^{-5}$ |
| $k = 16$ | 3.4×10^{-4} | $2900 t - 1.3 \times 10^{-4}$ |
| $k = 16 \dagger$ | 1.1×10^{-5} | $9.1 \times 10^4 t - 3.9 \times 10^{-3}$ |
| $k = 32$ | 7.7×10^{-7} | $1.3 \times 10^6 t - 5.9 \times 10^{-2}$ |
| $k = 32 \dagger$ | 8.8×10^{-10} | $2.4 \times 10^7 t - 1.0$ |

(\dagger = with 20% incoherent background)

Table 1: Rare events

domain configurations (varying k , fraction of incoherent corruption, and field strengths for $k=2$). Also included are upper bound expressions for the p_k 's.

From this data, we can conclude that the fraction of events lying in the tail falls off exponentially with k . Figure 6 shows a fit to the form

$$P_{\text{tail}} = A e^{-Bk} . \quad (31)$$

with fitted values $A = 0.147$ and $B = 0.370$. From this, it is estimated that k could increase to 40 before the number of tail events would be comparable to the incoherent case. Similarly, with 20% incoherent background included, $A = 0.20$, $B = 0.61$, and k can still increase to around 25 before the number of tail events would be comparable to the purely incoherent case.

6 Conclusion

We have conducted a detailed numerical investigation of multiple domains of disoriented chiral condensate. Although the dynamics of domain formation in the wake of a heavy ion

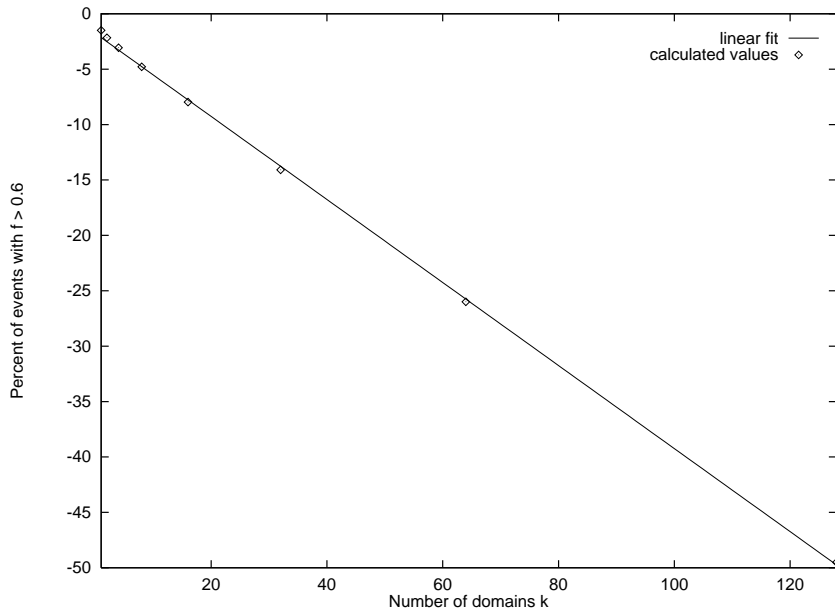


Figure 6: Tail events versus k

collision is far from completely understood, it is plausible that multiple domains are more likely to occur than a single coherent domain. We have concentrated on the evolution of multiple domains after formation, using the chiral lagrangian as a long-wavelength approximation for the dynamics. Our simulations follow the pion fields out to asymptotic distances, where we can characterize the number of particles per isospin and momentum bin that would be detected in an experiment. In choosing the initial conditions for our configurations, we opted for simplicity in neglecting important factors such as the expansion velocities. Given a particular dynamical model of the formation process, this could easily be incorporated into our simulations.

For small amplitudes, corresponding to low number densities of pions in the semi-classical fields, a simple statistical analysis suffices to characterize the isospin fluctuations of multiple domains (see figure 1). However, as the field strengths are increased, we see ample evidence of nonlinear behavior and significant interaction between domains. These nonlinear effects are already present for field strengths of order $\sim F_\pi$. For the case of two domains ($k = 2$), we were able to compute the effects of interactions on the probability distribution of isospin fluctuations (figure 2). While the shape of the curve is changed somewhat from the weak-field case, the probability of rare events (in particular, where f is close to unity) and the width of the distribution are not strongly affected. We suspect that the rare events with large f will prove to be the most robust signal of DCCs, surviving even multiple domain formation and large field strengths. Some interesting phenomena were observed in the evolution with

high initial field strengths. Relatively long-lived ‘breather’ or ‘pseudo-bound state’ configurations were found, in which the pions remained trapped on timescales many times larger than the light-crossing time of the initial configurations. In future work we hope to understand their dynamics better, as well as the prospects for their detection through correlation measurements.

Computational limitations prevented us from performing complete investigations of the case of $k > 2$. While we can perform individual runs, the time required to compute the associated probability distribution for f was prohibitive. Nevertheless, for the simplified cylindrical configurations we considered it is plausible that the $k = 2$ case captures the correct qualitative behavior for larger numbers of domains, as in any individual run the evolution is seen to be dominated by nearest domain interactions. Our results suggest that even events with a large number of small domains are capable of providing a detectable signature. We are hopeful that analysis of future RHIC data will allow stringent upper bounds to be placed on the probabilities of multiple domain formation, or alternatively the discovery of coherent phenomena in heavy ion collisions.

The authors would like to thank John Harris, Rudy Hwa, Vincent Moncrief, Krishna Rajagopal and Dirk Rischke for useful discussions and comments. Nick Evans and Stephen Selipsky are acknowledged for early participation in this project. This work was supported in part under DOE contracts DE-AC02-ERU3075 and DE-FG06-85ER40224.

7 Appendix A : Relations Between π and ϕ Fields

The ϕ and π fields are related via

$$\phi_0 + i\vec{\tau} \cdot \vec{\phi} = F_\pi e^{i\vec{\pi} \cdot \vec{\tau} / F_\pi} . \quad (32)$$

Using the identity

$$e^{i\vec{A} \cdot \vec{\tau}} = \cos(|A|) + i \frac{\vec{A} \cdot \vec{\tau}}{|A|} \sin(|A|) \quad (33)$$

we can write out the above equation

$$\phi_0 + i\vec{\tau} \cdot \vec{\phi} = F_\pi \cos\left(\frac{|\pi|}{F_\pi}\right) + iF_\pi \frac{\vec{\pi} \cdot \vec{\tau}}{|\pi|} \sin\left(\frac{|\pi|}{F_\pi}\right) \quad (34)$$

which implies

$$\phi_0 = F_\pi \cos\left(\frac{|\pi|}{F_\pi}\right) \quad (35)$$

and

$$\vec{\phi} = F_\pi \frac{\vec{\pi}}{|\pi|} \sin\left(\frac{|\pi|}{F_\pi}\right) . \quad (36)$$

By inverting the equation for ϕ_0 above, we get

$$|\pi| = F_\pi \arccos\left(\frac{\phi_0}{F_\pi}\right) , \quad (37)$$

and since $\vec{\pi}$ and $\vec{\phi}$ point in the same direction (as seen from the equation solving for $\vec{\phi}$ above), we get

$$\vec{\pi} = F_\pi \arccos\left(\frac{\phi_0}{F_\pi}\right) \frac{\vec{\phi}}{|\phi|} . \quad (38)$$

However, this will not suffice for the case where the values of the ϕ fields are approximated. The problem is that there are four ϕ fields while there are only three π 's. The reason that this is possible is because there is an implicit condition on the ϕ 's – that $\phi^2 \equiv \phi_0^2 + \vec{\phi}^2 = 1$. If this is broken even slightly, it is possible that $\phi_0 > F_\pi$, and then $\cos^{-1}(\frac{\phi_0}{F_\pi})$ becomes imaginary.

To avoid this problem, a fourth parameter is coupled with the π 's, a K field that measures the length of ϕ ($K^2 = \phi^2$). Using this, equations 35 and 36 become

$$\phi_0 = K \cos\left(\frac{|\pi|}{F_\pi}\right) \quad (39)$$

$$\vec{\phi} = K \frac{\vec{\pi}}{|\pi|} \sin\left(\frac{|\pi|}{F_\pi}\right) . \quad (40)$$

Inverting these yields

$$K = |\phi| , \quad (41)$$

and

$$\vec{\pi} = F_\pi \arccos\left(\frac{\phi_0}{|\phi|}\right) \frac{\vec{\phi}}{|\phi|} . \quad (42)$$

Now we can assume that $K \simeq F_\pi$ and throw away the information in K .

8 Appendix B : The Particle Detector

The number of particles can be detected by using the usual Klein-Gordon number operator in the limit of the simulation where the wave is dispersed and the nonlinearities have become negligible. The number operator is

$$N = \frac{1}{(2\pi)^3} \int d^3\vec{p} a_{\vec{p}}^\dagger a_{\vec{p}} . \quad (43)$$

As we are in the classical limit, we can treat all these operators as c-numbers and simply solve the above in terms of the fields. To do this we start with

$$\pi(x) = \int \frac{d^3\vec{p}}{(2\pi)^3} \frac{1}{\sqrt{2E_{\vec{p}}}} (a_{\vec{p}} e^{-i p \cdot x} + a_{\vec{p}}^\dagger e^{i p \cdot x}) . \quad (44)$$

After some algebra, this equation can be inverted to solve for a , yielding

$$a_{\vec{p}} = \frac{1}{\sqrt{2}} e^{iE_{\vec{p}}t} \int d^3\vec{x} \left(\sqrt{E_{\vec{p}}} \pi(x) + i\sqrt{\frac{1}{E_{\vec{p}}}} \dot{\pi}(x) \right) e^{-i \vec{p} \cdot \vec{x}} \quad (45)$$

$$= \frac{1}{\sqrt{2}} e^{iE_{\vec{p}}t} \text{FT}_{\vec{p}} \left[\sqrt{E_{\vec{p}}} \pi(x) + i\sqrt{\frac{1}{E_{\vec{p}}}} \dot{\pi}(x) \right] . \quad (46)$$

It might seem natural to simply insert this into the definition of N and derive an explicit expression. However complexities arise due to the non-local nature of the N operator. Hence, we separately calculate the $a_{\vec{p}}$ field then use this to obtain N .

Two useful equations are those of the Fourier transform in axial and spherical coordinates, given by the spherically symmetric case

$$\text{FT}(P_r)[f(r)] = \int d^3\vec{x} f(r) e^{-i \vec{x} \cdot \vec{p}} = 4\pi \frac{1}{p_r} \int_0^\infty dr f(r) r \sin(rP_r) \quad (47)$$

and the axially symmetric case

$$\text{FT}(P_r, P_z)[f(r, z)] = \int d^3\vec{x} f(r, z) e^{-i \vec{x} \cdot \vec{p}} = 2\pi \int_0^\infty \int_{-\infty}^\infty dz dr f(r) r J_0(rP_r) e^{-i zP_z} . \quad (48)$$

In addition to its use in calculating the number of particles, transforming to momentum space allows us to inspect against possible aliasing problems. Because of the axial (or spherical) symmetry and complicated shapes involved, this would be difficult to do analytically. However, a plot of a_p vs. $|p|$ (for representative values of \vec{p}) can be visually checked. As in one dimensional Fourier Transformations, discretization copies the primary Fourier transformed image centered around zero momentum in a repeating pattern at higher frequencies (albeit deformed). By viewing a_p we insure that each copy decays fast enough as to not interfere with its neighbor. Figure 7 shows a sample a_p , which can visually be seen to decay before the second image (which is not shown).

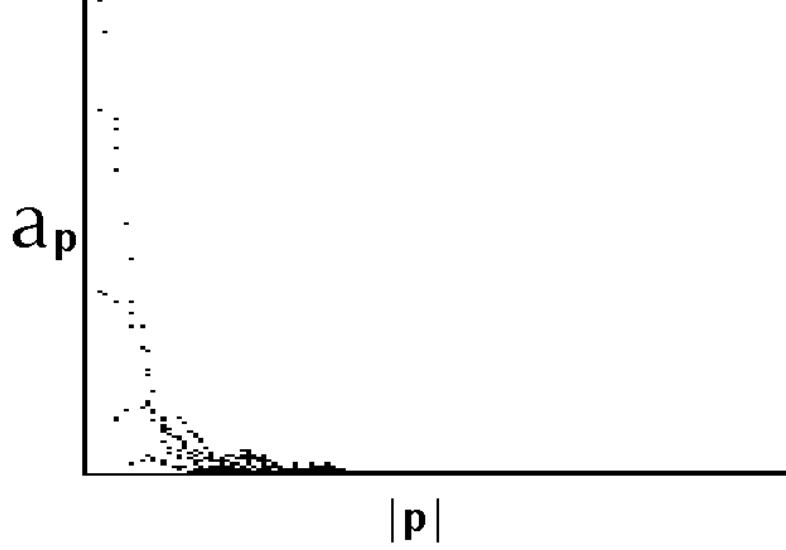


Figure 7: An example of typical values for a_p vs. $|p|$

9 Appendix C : Rotating the Configuration

To minimize the number of simulation runs, we used the results of one run to calculate the detected pion distributions resulting from initial conditions which differ from those of the first run by a rotation in isospin space. The definition of the Klein-Gordon number operator is

$$N = \frac{1}{(2\pi)^3} \int d^3\vec{p} a_{\vec{p}}^\dagger a_{\vec{p}} . \quad (49)$$

In our case we have three associated number operators, for $\pi_{0,+,-}$:

$$N^j = \frac{1}{(2\pi)^3} \int d^3\vec{p} (a_{\vec{p}}^j)^\dagger a_{\vec{p}}^j . \quad (50)$$

An isospin rotation on the configuration yields a new set of a_j 's via the usual transformation,

$$\tilde{a}^j = R_{j'}^j a^{j'} , \quad (51)$$

where R is a 3×3 $SO(3)$ matrix. Applying this to the N_i 's, one obtains an expression involving cross terms $(a^j)^\dagger a^k$, so a new tensor is introduced

$$N^{j,k} = \frac{1}{(2\pi)^3} \int d^3\vec{p} (a_{\vec{p}}^j)^\dagger a_{\vec{p}}^k , \quad (52)$$

where the single indexed N^i 's are just the diagonal elements of the double indexed $N^{j,k}$,

Now the N 's can be trivially rotated via the usual tensor rotation law,

$$\tilde{N}^{j,k} = R_{j'}^j R_{k'}^k N^{j',k'} . \quad (53)$$

10 Appendix D : Computational Technique

Besides initial configurations, each numerical simulation had a series of internal parameters, whose values were independent of the physics of the problem but needed to be determined in order to insure proper results were obtained. These parameters included the spatial discretization Δx , time step Δt , total evolution time T , and linear sigma potential scaling λ .

Of these, Δx and Δt proved to be quite simple to fix, as the final results were insensitive to the chosen values, aside from cases where evolution became obviously unstable. Chosen $(\Delta x, \Delta t)$'s within the stable region yielded final values which agreed within reasonable errors, so for a given Δx , the coarsest stable value of Δt was chosen, thus decreasing needed computational power. It should be noted that the required Δt decreased as field strength and λ were increased to high values, because when this is done, higher frequency oscillations become more dominant in the evolution.

A reasonable value of λ was found by holding everything else fixed, then calculating and plotting the number operator for varying λ (see figure 8). From this plot we were able to visually pick out the convergence point of the curve. The curve converges for values of λ in the hundreds, but as the computational cost of raising λ turned out to be low, the much more conservative value of $\lambda = 6000$ was chosen.

The remaining parameter, evolution time T , proved to be the least straightforward to work with. In principle the same technique was used as for λ , but in practice difficulties resulted due to the large and sudden variation in decay time for differing initial conditions (see section 4.3 for details of this phenomenon). Longer evolution times stretched the limits of our machines' memory and processor speed, and in the end were the deciding factor in limiting initial field strengths less than or equal to $1.6 F_\pi$. Figure 9 shows a typical plot of calculated N versus T illustrating how the convergence process took place.

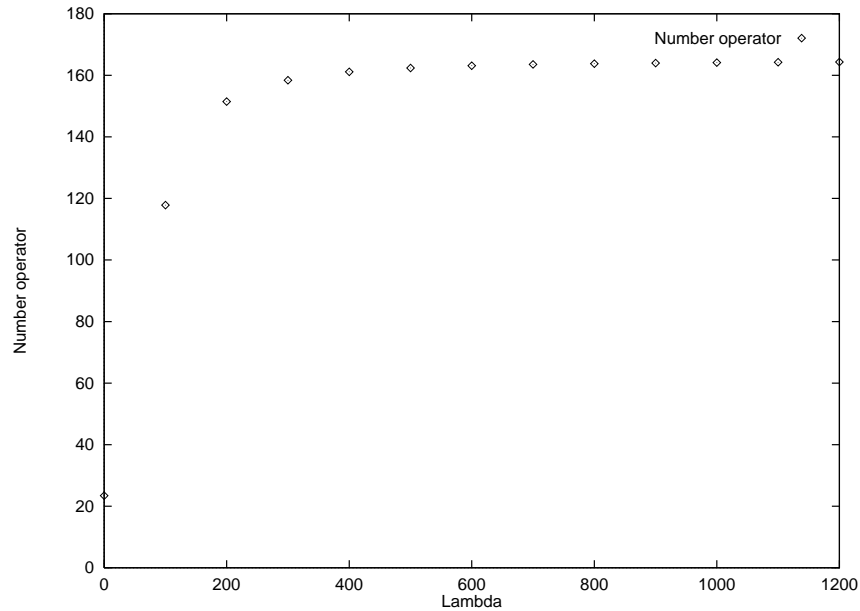


Figure 8: Number operator vs. λ

References

- [1] A.A. Anselm, Phys. Lett. B217 (1989) 169.
- [2] A.A. Anselm and M.G. Ryskin, Phys. Lett. B266 (1991) 482.
- [3] J.-P. Blaizot and A. Krzywicki, Phys. Rev. D46 (1992) 246.
- [4] K. Rajagopal and F. Wilczek, Nucl. Phys. B399 (1993) 395.
- [5] J.D. Bjorken, K.L. Kowalski, and C.C. Taylor, 7th Les Rencontres de Physique de la Vallee d'Aoste: Results and Perspectives in Particle Physics, La Thuile, Italy, 7-13 Mar 1993; Report SLAC-PUB-6109 (1993).
- [6] K. Rajagopal, in *Quark-Gluon Plasma 2*, ed. R. Hwa, World Scientific (1995).
- [7] J.-P. Blaizot and A. Krzywicki, Acta Phys. Polon. 27 (1996) 1687
- [8] K. Rajagopal and F. Wilczek, Nucl. Phys. B404 (1993) 577.
- [9] S. Gavin, A. Gocksch, and R.D. Pisarski, Phys. Rev. Lett. 72 (1994) 2143.
- [10] Z. Huang and X.-N. Wang, Phys. Rev. D49 (1994) 4335.
- [11] S. Gavin and B. Müller, Phys. Lett. B329 (1994) 486.
- [12] J.-P. Blaizot and A. Krzywicki, Phys. Rev. D50 (1994) 442.
- [13] F. Cooper, Y. Kluger, E. Mottola, and J.P. Paz, Phys. Rev. D51 (1995) 2377.
- [14] D. Boyanovsky, H.J. de Vega, and R. Holman, Phys. Rev. D51 (1995) 734.

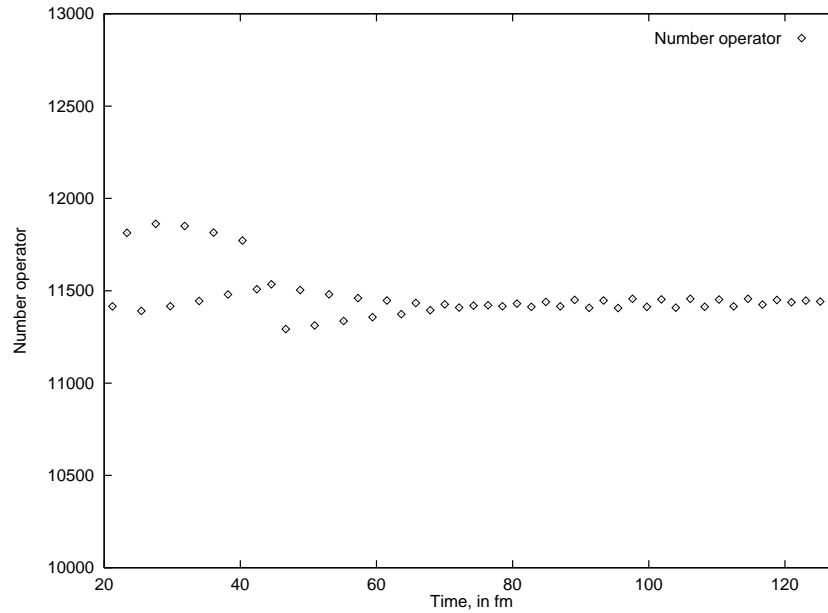


Figure 9: Number operator vs. evolution time

- [15] M. Asakawa, Z. Huang, and X.-N. Wang, Phys. Rev. Lett. 74 (1995) 3126.
- [16] L.P. Csernai and I.N. Mishustin, Phys. Rev. Lett. 74 (1995) 5005.
- [17] Y. Kluger, F. Cooper, E. Mottola, J.P. Paz, and A. Kovner, Nucl. Phys. A590 (1995) 581c.
- [18] S. Mrówczyński and B. Müller, Phys. Lett. 363B (1995) 1.
- [19] J. Randrup, Phys. Rev. Lett. 77 (1996) 1226; Nucl. Phys. A616 (1997) 531.
- [20] See, e.g., *Weak Interactions and Modern Particle Theory*, H. Georgi, Benjamin/Cummings, 1984.
- [21] R.D. Amado and Yang Lu, Phys. Rev. D54 (1996) 7075.
- [22] S. Pratt, in *Quark-Gluon Plasma 2*, ed. R. Hwa, World Scientific (1995).